Title

Acidic Methanol Treatment Facilitates Matrix-Assisted Laser Desorption Ionization-Mass Spectrometry Imaging of Energy Metabolism.

Journal

Analytical Chemistry, 95(40)

Authors

Jankowski, Connor
Samarah, Laith
McReynolds, Melanie
et al.

Publication Date

2023-10-10

DOI

10.1021/acs.analchem.3c01875

Peer reviewed

analytical chemistry

pubs.acs.org/ac
Article

Acidic Methanol Treatment Facilitates Matrix-Assisted Laser Desorption Ionization-Mass Spectrometry Imaging of Energy Metabolism

Wenyun Lu,* Noel R. Park, Tara TeSlaa, Connor S.R. Jankowski, Laith Samarah, Melanie McReynolds, Xi Xing, Jessica Schembri, Morgan T. Woolf, Joshua D. Rabinowitz, and Shawn M. Davidson*

Cite This: *Anal. Chem.* 2023, 95, 14879−14888

ABSTRACT: Detection of small molecule metabolites (SMM), particularly those involved in energy metabolism using MALDI-mass spectrometry imaging (MSI), is challenging due to factors including ion suppression from other analytes present (e.g., proteins and lipids). One potential solution to enhance SMM detection is to remove analytes that cause ion suppression from tissue sections before matrix deposition through solvent washes. Here, we systematically investigated solvent treatment conditions to improve SMM signal and preserve metabolite localization. Washing with acidic methanol significantly enhances the detection of phosphate-containing metabolites involved in energy metabolism. The improved detection is due to removing lipids and highly polar metabolites that cause ion suppression and denaturing proteins that release bound phosphate-containing metabolites. Stable isotope infusions of [$^{13}C_6$]nicotinamide coupled to MALDI-MSI ("Iso-imaging") in the kidney reveal patterns that indicate blood vessels, medulla, outer stripe, and cortex. We also observed different ATP:ADP raw signals across mouse kidney regions, consistent with regional differences in glucose metabolism favoring either gluconeogenesis or glycolysis. In mouse muscle, Iso-imaging using [$^{13}C_6$]glucose shows high glycolytic flux from infused circulating glucose in type 1 and 2a fibers (soleus) and relatively lower glycolytic flux in type 2b fiber type (gastrocnemius). Thus, improved detection of phosphate-containing metabolites due to acidic methanol treatment combined with isotope tracing provides an improved way to probe energy metabolism with spatial resolution *in vivo*.

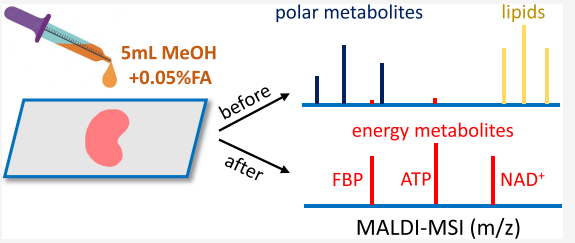

INTRODUCTION

Spatially resolved metabolomics aims to quantify small-molecule metabolites (SMMs) and lipids from tissues and holds the potential to characterize alterations in metabolic processes occurring in health and disease.[1] Obtaining anatomical metabolite measurements using conventional liquid chromatography-mass spectrometry (LC−MS)-based methods requires physical microdissection of tissues of interest followed by metabolite extraction and analysis from the individual areas.[2] For example, Ding et al. performed metabolomic analysis for 1547 metabolites across 10 mouse brain regions.[3] Another study employed a microarray collection system to dissect mouse brain areas with a resolution of 0.125 mm^3 and generated maps for 79 metabolites.[4] The other more commonly used approach is mass-spectrometry imaging (MSI) coupled with ionization techniques such as matrix-assisted laser desorption ionization (MALDI) and desorption electrospray ionization (DESI), or secondary ion mass spectrometry (SIMS).[1,5,6] The developments of MALDI-MSI platforms with a high mass resolving power have enabled the quantification of unlabeled and labeled metabolites, facilitating critical measurements, such as determining the spatially resolved nutrient contribution to metabolic pathways and flux analysis.[7−10]

Despite progress in this area, overall metabolite coverage using MALDI is limited compared to commonly used chromatography-based metabolomics methods. We hypothesized that metabolome coverage could be improved by reducing ion suppression from other analytes and removing physiological salts. Ion suppression during MALDI occurs from a combination of other analytes, including proteins, matrix compounds, salts, and analytes with high ionization efficiency (IE) or are present in high abundance. Additionally, the physiological pH and salt concentration influence the charge state and, therefore, ionization efficiency of individual analytes in a biological sample. To improve sensitivity for other classes of analytes, such as lipids and proteins, procedures have been developed to remove undesired analytes that cause ion suppression. Previous results have demonstrated that "washing" prepared samples with

Received: May 1, 2023
Accepted: August 15, 2023
Published: September 27, 2023

https://doi.org/10.1021/acs.analchem.3c01875
Anal. Chem. 2023, 95, 14879−14888

organic solvents can remove lipids and salts, enhancing the signal of desired analytes.[11−14] Treatment with organic solvents such as chloroform or acetone for SMM detection is also beneficial.[15,16] Washing with aqueous solvents, such as ammonium formate at pH 6.4 improved lipid detection and coverage.[17]

Isotope tracing experiments bring additional challenges as the metabolite labeling fraction is typically at 1−25%,[9,18] which necessitates improving SMM detection while maintaining anatomical tissue structure. Here, we systematically investigated the effect of washing with a broad range of solvents on SMM detection using MALDI. We found that chloroform is an effective solvent for removing lipids and improving SMM signals for multiple mouse tissues, consistent with previous results.[15] More importantly, washing with acidic methanol has a surprising effect that only enhances the signal predominantly for phosphate-containing metabolites, many of which are involved in energy metabolism. The improved sensitivity we observe is at least in part because of a combination of the removal of lipids and highly polar metabolites, including amino acids and hexose, and the denaturing of proteins. Additional method optimization was performed, and we arrived at the optimal washing procedure, which involves pipetting 1 mL of MeOH + 0.05% formic acid (5 times) over tissue slides, followed by matrix coating using *N*-(1-naphthyl)ethylenediamine dihydrochloride (NEDC) or 2′,4′,6′-trihydroxyacetophenone (THAP) as matrices in negative and positive mode, respectively. This washing procedure reveals distributions of ATP (adenosine triphosphate) relative ADP (adenosine diphosphate) signal in the mouse kidney. In addition, combined with ^{13}C-isotope tracer infusions, we observed region-specific NAD^+ (nicotinamide adenine dinucleotide) synthesis in mouse kidney and glycolytic activity in mouse muscles.

EXPERIMENTAL SECTION

Wash Procedures and Sample Preparation. Serial sections of mouse tissues at a thickness of 10 μm were acquired using a cryostat (Leica CM3050S, Wetzlar, Germany) and thaw-mounted on indium tin oxide (ITO)-coated glass slides (Bruker Daltonics, Bremen, Germany) for MALDI analysis or mounted on standard glass slides for H&E when needed. Tissue slides were desiccated under vacuum for 10 min and underwent solvent wash before matrix application. Two wash procedures were tested (beaker vs pipetting, Figure S1).

(1) "Beaker:" this procedure is adapted from Yang *et al.,* in which tissue slides were immersed into 25 mL solvent in a 25 mL glass beaker for 30 s.[15] At the end of the wash, the residual solvent was tapped off by incline, and the slide was desiccated again for 5 min before matrix application. This procedure was used in the initial screening of 13 solvent wash conditions.

(2) "Pipetting:" this procedure, adapted from Lemaire *et al.*, involves placing the tissue slide on an incline and pipetting solvents over the tissue surface.[11] Either a 1 mL pipette tip or 5 mL serological pipette was tested, and the former gave more consistent results, and 5 × 1 mL solvent was used as the final wash condition. The slide was desiccated again for 5 min before matrix application (see the Supporting Information for details of matrix coating).

MALDI Imaging. MALDI image runs were performed on a solariX XR FT-ICR mass spectrometer with a 9.4 T magnet (Bruker Daltonics, Bremen, Germany). The instrument was calibrated using arginine solution at 1 mg/mL before the run and calibrated using lock masses during the run with an intensity threshold of 5e5. Data were collected in two different scanning modes targeting different m/z windows. We used full scan mode covering m/z 100−800 for broad metabolite coverage with a resolving power of 120,000 at m/z 500, laser power at 20%, laser focus set as "small," and x-y raster width of 50 μm. We used the cumulative accumulation of selected ions mode (CASI) to cover a narrow m/z window for more specific metabolite coverage. Samples were run with an x-y raster width of 20 μm for better spatial resolution, with laser power at 22%, laser focus set as "minimum." A spectrum was accumulated from 200 laser shots at 1200 Hz.

Data Analysis and Metabolite Annotation. Data were analyzed using IsoScope (https://github.com/xxing9703/Isoscope). In brief, the metabolites were identified using high-resolution accurate mass with a ppm window of 10 ppm compared to an in-house metabolite list established on liquid chromatography-mass spectrometry (LC−MS) using authenticated standards.[19−21] We used a list of ∼100 metabolites in negative ion mode for the initial screen of different wash methods from a previous report.[8] We later expanded the list to include 175 and 80 compounds in negative and positive modes, respectively. The majority of metabolites were detected in the $[M + H]^+$ state in positive mode and $[M\text{-}H]^-$ state in negative mode, with a few metabolites in adduct form (e.g., hexose-Cl^- at m/z 215.03279 in negative mode). In addition, MS/MS spectra were collected to confirm the selected metabolites' identity.

RESULTS

Initial Screening Wash Conditions. The topological composition of macromolecules in specific organs and anatomical regions (e.g., protein-rich, lipid-rich areas of the brain) presents regional ion-suppression challenges. We hypothesized that lipids, which ionize well by MALDI and are highly abundant, would be one primary source of ion suppression. We designed an experiment to test whether altering the composition of tissues using washes of solvents with varying polarity could increase the ion signal of small molecule metabolites of interest. We started with 13 solvents with different physical and chemical properties (Table S1), including common organic solvents (cyclohexane, hexane, toluene, methyl *t*-butyl ether (MTBE), tetrahydrofuran (THF), ethyl acetate, chloroform, pyridine, dichloromethane, acetone, 2-propanol (IPA), ethanol, as well as a solvent that we routinely used for metabolite extraction from tissues (40% acetonitrile: 40% methanol: 20% water: 0.5% formic acid (FA), simplified as 404020FA).[22,23]

Detection of Polar Metabolites. Using a previously reported metabolite list,[8] we detected 94 and 101 polar metabolites in negative ionization mode across all conditions from the mouse brain and kidney, respectively. We added 41 lipid species by matching the detected m/z from separate runs using LC−MS. Signals were averaged over the same tissue region, and the ratio was calculated after wash versus before wash (Table S2). Following the wash procedure, we observed an inverse correlation between lipid and polar metabolite signals (Figure S2). This inverse correlation is more robust for polar metabolites detected in the brain than polar metabolites detected in the kidney, likely because the brain has higher lipid content.[24] In general, this is consistent with previous results showing that washing with chloroform or acetone helps to improve polar metabolite detection by reducing ion suppression

https://doi.org/10.1021/acs.analchem.3c01875
Anal. Chem. 2023, 95, 14879−14888

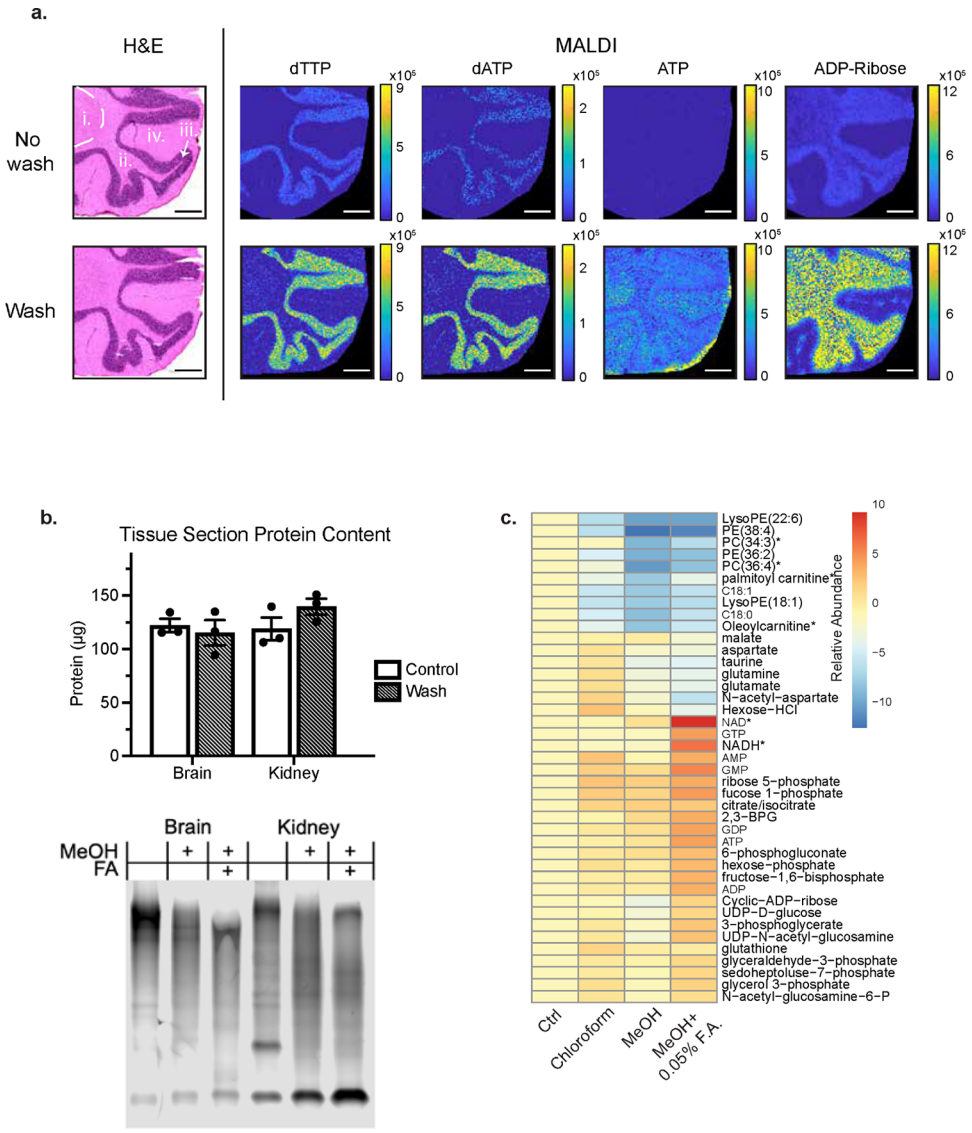

Figure 1. Treatment of tissue section with MeOH + 0.05% FA maintains the histological morphology, denatures protein, removes lipids and highly polar metabolites, and improves the detection of phosphate-containing energy metabolites. (a) H&E images and MALDI images of selected metabolites (dTTP, dATP, ATP, ADP-ribose) before and after wash with 5 mL of MeOH + 0.05% FA demonstrate the histological morphology is maintained and metabolites are not moving. MALDI experiment was performed with a raster size of 20 μm. Anatomical regions are denoted as (i) deep cerebral nuclei, (ii) white matter, (iii) granule cell layer, and (iv) molecular layer. Scale bar = 500 μm. (b) Quantification of protein from serial sections of a kidney using bicinchoninic acid (BCA) assay. Running quantified protein on a native gel reveals no total protein content change (n = 3 tissue per condition) before and after wash with MeOH + 0.05% FA. While proteins are not being washed away, Coomassie blue staining of protein lysates from control and washed tissue sections separated by Native PAGE shows that lysates from tissues washed with methanol displayed increased mobility, and the effect was augmented by the inclusion of formic acid (FA), suggesting that proteins from washed samples are denatured. (c) Heatmap of selected compounds across four different wash conditions ($\log_2$ fold of change): no wash control, 5 mL of chloroform, 5 mL of MeOH, 5 mL of MeOH + 0.05% FA. Compounds marked with * are detected in positive mode with a THAP matrix, while all other compounds are detected in negative mode with an NEDC matrix. Chloroform removes lipids and increases signals for polar metabolites. MeOH also removes lipids and selected highly polar metabolites such as taurine, glutamine, and glutamate while improving the signal of other polar metabolites. MeOH + 0.05% FA removes lipids and highly polar metabolites while enhancing the detection of phosphate-containing energy metabolites.

from lipids.[15] Among all solvents investigated, chloroform shows the best overall signal enhancement for polar metabolites, with a median fold increase of 2.54 and 1.68 for polar metabolites in the brain and kidney, respectively (Figure S2).

Acidic Methanol Wash Improves the Detection of Phosphate-Containing Energy Metabolites and Is Compatible with NEDC for Analysis in Negative Ionization. Among the 13 solvents investigated, 404020FA appears unique as the median folds of difference after washing are close to one for both lipids and polar metabolites (Figure S2). Many highly polar metabolites were depleted after washing, including amino acids and derivatives such as taurine, glutamine, glutamate, and hexose (detected as Cl^- adduct; Table S3). Examination of the metabolite images of taurine, glutamine, glutamate, and Hexose-Cl^- yields contrasting images in the 404020FA samples compared to the control, indicating that the observed pattern is what is left over after wash, as the majority of these metabolites are washed away. In contrast, for other wash conditions, the spatial patterns are roughly maintained (Figure S3).

https://doi.org/10.1021/acs.analchem.3c01875
Anal. Chem. 2023, 95, 14879−14888

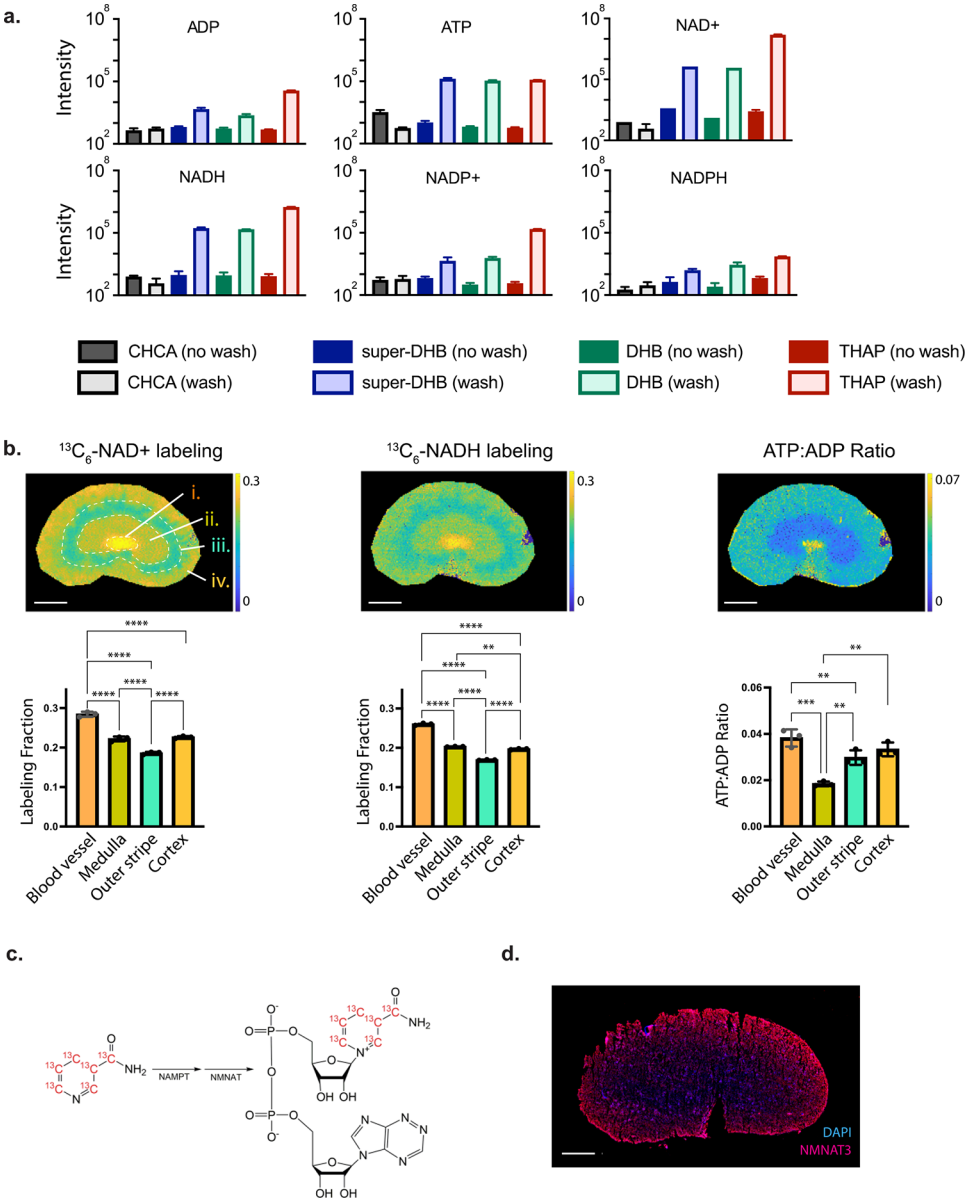

Figure 2. Acidic methanol treatment enables the detection of ADP, ATP, NAD^+, NADH, $NADP^+$, and NADPH in positive mode, revealing relative ATP and ADP signal across mouse kidney, as well as NAD^+ and NADH synthesis from [$^{13}C_6$]nicotinamide infusion. (a) Signal of ADP, ATP, NAD^+, NADH, $NADP^+$, and NADPH from mouse kidney before and after wash with 5 mL of MeOH + 0.05% FA, using four different matrices: CHCA, DHB, super-DHB, and THAP. (b) Upon infusion with [$^{13}C_6$]nicotinamide (NAM), NAD^+, and NADH get labeled, and the [$^{13}C_6$] labeling ratio shows a pattern that distinguishes blood vessels (i), medulla (ii), outer stripe (iii), and cortex (iv) (n = 3 technical replicates). ATP relative to ADP raw signal (calculated from raw ion counts, thus not the actual concentration ratio) varies across different regions. Statistical analyses were performed using GraphPad Prism software. $^{**}p$ value < 0.05; $^{***}p$ value < 0.005, $^{****}p$ value < 0.0005. Scale bar 2 mm. (c) Schematic of the NAD^+ synthesis pathway from [$^{13}C_6$]nicotinamide (NAM). NAD^+ then converts to NADH through a reduction reaction. (d) Immunofluorescence of 4′,6-diamidino-2-phenylindole (DAPI, as a control) and NMNAT3 in kidney cross section shows that NMNAT3 expression is highest in cortex region. Scale bar: 1 mm.

While this highly polar solvent fails to remove lipids as efficiently as highly nonpolar solvents tested (e.g., chloroform), careful examination of data on polar metabolites shows improved detection for different compound classes. Detection of many phosphate-containing energy metabolites was enhanced, including glycolytic intermediates 3-phosphoglycerate (3-PG), hexose 6-phosphate (hexose-6P), and fructose 1,6-bisphosphate (FBP) as well as nucleotide phosphates adenosine monophosphate (AMP), ADP, and ATP (Table S3). To determine which components of 404020FA are responsible for the observed effect, we examined serial section of the mouse brain and kidney in eight different solvent conditions: acetonitrile, acetonitrile + 0.5% FA, methanol, methanol + 0.5 %FA, 404020, 404020 + 0.5% FA, H_2O, and H_2O + 0.5% FA. The results demonstrate that combining methanol with formic acid is responsible for the observed effect (e.g., the enhancement of the signal intensity for 3-PG, hexose-6-phosphate, FBP, AMP, ADP, and ATP) (Table S4).

After identifying acidic methanol wash as an effective way to enhance energy metabolite detection, a series of experiments were performed to optimize the wash procedure. We first explored the possibility of washing using "pipetting" (Figure S1). Instead of dipping the tissue slide into a beaker with 25 mL solvent, which requires a relatively large solvent volume, the

https://doi.org/10.1021/acs.analchem.3c01875
Anal. Chem. 2023, 95, 14879−14888

pipetting procedure involves placing the tissue slide on an incline and pipetting a small amount of solvent over the tissue surface.[11] Experiments were performed using 2, 4, 8, and 16 mL of MeOH + 0.5% FA with results on 3-PG, Hexose-6P, FBP, AMP, ADP, and ATP shown in Figure S4. AMP signal peaks at 2 mL and then decreases with increasing washing volume, likely because it is being washed away from tissue sections. The results for the other five compounds were similar for different solvent volumes.

We also studied the use of formic acid at lower concentrations. Experiments were performed using 2, 4, and 6 mL of MeOH + 0.05% FA and 2, 4, and 6 mL of MeOH + 0.1% FA on the kidney. For the six compounds shown in Figure S5, signal enhancements upon washing are similar across tested conditions, suggesting that a range of formic acid concentrations and solvent volumes generates similar results. Additional experiments were performed using 5 mL of MeOH + 0.05% FA to test for any tissue anatomy change from the cerebellum region (sagittal) after wash. H&E shows that tissue anatomy was conserved. MALDI data on selected metabolites of dTTP, dATP, ATP, and ADP-ribose show that their spatial distribution was also maintained (Figure 1a). Thus, 5 mL of MeOH + 0.05% FA was chosen as the final wash condition. For other tissues, systematic work is needed to evaluate tissue-specific wash conditions, such as types of acids (e.g., formic acid, acetic acid, trifluoroacetic acid), acid concentrations, solvent volumes, types of matrices, and matrix spraying conditions. In doing so, evaluating whether different wash procedures cause metabolite delocalization is critical.

What is the underlying reason for the enhancement of phosphate-containing metabolite signal? We hypothesized that along with lipids, high levels of endogenous protein or peptides may cause ion suppression. Measuring protein concentration before and after washing shows the total protein content did not change (Figure 1b). This result suggested that endogenous protein levels are not the dominant source of ion suppression. We next hypothesized that acidic methanol may alter that protein conformation, specifically by denaturing proteins and disrupting protein−metabolite interactions. Native PAGE on protein lysates from control and washed tissue sections show that lysates from tissues washed with methanol displayed increased mobility, suggesting that proteins from washed samples are denatured. Wash with MeOH + FA increased mobility further, indicating that MeOH + FA more effectively denatures proteins than MeOH alone (Figure 1b, Figure S6). Many phosphate-containing metabolites—for example, ATP and $NADP^+$—bind to proteins.[25,26] It is possible that once proteins are denatured, metabolites are released and become detectable. In addition, the mass spectra data from tissue washed with MeOH + 0.05% FA shows that this solvent removes lipids, and highly polar metabolites, including amino acids and hexose (Figure 1c, Figure S7). The removal of these specific compounds is confirmed by LC−MS analysis of the post-wash solvents (Figure S8). In sum, it is probable that the combination of these three factors, i.e., denaturing proteins, removal of lipids, and removal of highly polar metabolites contributes to the improved detection of phosphate-containing metabolites.

The improved detection for many phosphate-containing metabolites expands detected SMMs to 175 compounds in negative mode using NEDC as a matrix, including 134 polar metabolites and 41 lipids (Table S5). On-tissue MS^2 was performed for 21 metabolites, and their identity was confirmed by comparing them with the library MS^2 spectrum (Table S6). Additional experiments were performed using mouse brain, kidney, spleen, muscle, and heart to investigate metabolite detection under different wash conditions with 5 mL of chloroform, methanol, and MeOH + 0.05% FA (Table S7), providing a valuable resource for signal enhancement of individual metabolites under different wash conditions in a tissue-specific manner.

Detection of ADP, ATP, NAD^+, NADH, $NADP^+$, and NADPH in Positive Ionization Mode. Mono-, di-, and trinucleotides (e.g., AMP, ADP, ATP, NAD^+, NADH, $NADP^+$, and NADPH) are essential cofactors in many metabolic processes.[27−29] While AMP, ADP, ATP, NADH, and NADPH are detectable in negative mode with NEDC matrix after MeOH + 0.05% FA treatment (Table S7), NAD^+ and $NADP^+$ remained undetectable. LC−MS data on kidney tissue extract showed that positive ion mode generally results in higher signal than negative mode for these compounds (4-fold difference for NAD^+ signal) (Figure S9). Therefore, we further investigated several matrices that would be most compatible in positive ionization, including CHCA (α-Cyano-4-hydroxycinnamic acid), DHB (2,5-dihydroxybenzoic acid), super-DHB (mixture of 2,5-dihydroxybenzoic acid and 2-hydroxy-5-methoxybenzoic acid), and THAP (2′,4′,6′-trihydroxyacetophenone), after washing with MeOH + 0.05% FA for identical tissue sections. CHCA appeared to be a poor matrix for detecting nucleotide compounds, while the other three matrices (DHB, super-DHB, THAP) yielded an exceptional signal after washing. Using our optimized wash condition, combined with the best of the four matrices tested (THAP), we observed ∼1000-fold improvement in the detection of NAD^+ (Figure 2a). Visualizing metabolites such as NAD^+ highlights the importance of integrating acidic methanol treatment and selecting the suitable matrix for metabolite detection.

For nucleotide phosphates, we rely on the accurate mass within ±5 ppm m/z window for identification. We further confirmed the identity using on-tissue MS^2 fragmentation of NAD^+ (Table S6). However, we could not isolate sufficient NADH to generate an MS^2 fragmentation pattern. Another possible way to validate the identities of NAD^+ and NADH is to perform an *in vivo* isotope tracing study using $^{13}C_6$-nicotinamide (NAM), one of the main precursors of NAD^+ and NADH synthesis.[30−32] We infused free-moving conscious mice with $^{13}C_6$-NAM for 8 h, a sufficient time for incorporation of ^{13}C-NAM into NAD^+ and NADH. LC−MS analysis of nicotinamide in serum reveals a labeling ratio of 0.733 (±0.016, $n = 3$ technical replicates). LC−MS of the kidney section shows that NAD^+ and NADH are labeled in $^{13}C_6$-form at 0.209 (±0.004) and 0.182 (±0.006), respectively. We detected the $^{13}C_6$-NAD^+ and $^{13}C_6$-NADH ions from kidney section after acidic methanol treatment with THAP matrix with MALDI with comparable fractional labeling compared to LC−MS. These results further support the accurate measurement of NAD^+ and NADH using MALDI. Interestingly, we observed different labeling ratios of NAD^+ and NADH across distinct regions: blood vessels, renal medulla, outer stripe, and renal cortex, thus reflecting regional differences in their biosynthesis from circulating NAM (Figure 2b).

Since NAD^+ can be synthesized from NAM through multiple steps involving proteins nicotinamide phosphoribosyltransferase (NAMPT) and nicotinamide mononucleotide adenylyltransferase (NMNAT) (Figure 2c), we next examined enzyme expression that may explain the observed metabolite patterns. Immunofluorescence of the mitochondrial isoform NMNAT3 in the mouse kidney section shows that it is highly expressed in cortex (Figure 2d), which explains the relatively high labeling of

https://doi.org/10.1021/acs.analchem.3c01875
Anal. Chem. 2023, 95, 14879−14888

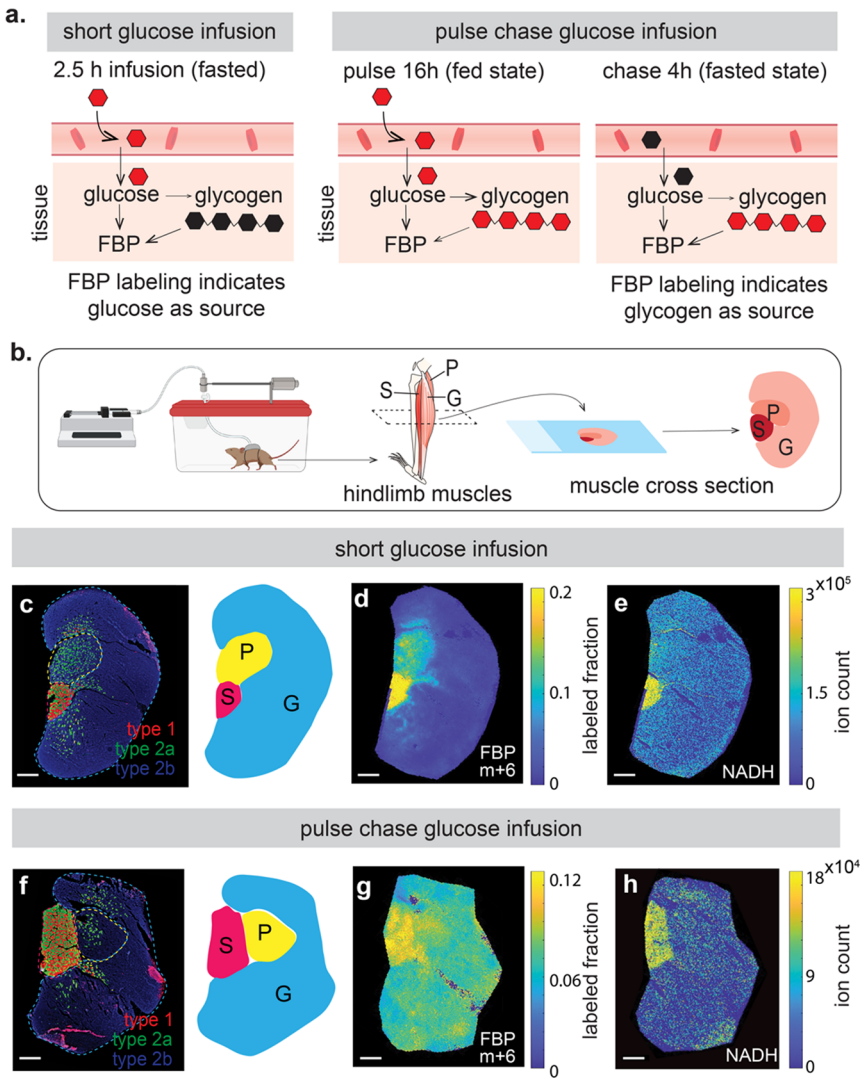

Figure 3. Differential glycolytic labeling in skeletal muscle fiber types is revealed by short glucose infusion and pulse-chase infusion coupled with an acidic methanol wash. (a) Schematic of isotope tracing experiments performed to determine the source of glycolytic intermediates in muscle. The panel on the left depicts a 2.5-hour infusion of [U-^{13}C]glucose to visualize the muscle regions that use glucose directly via labeling in glycolytic intermediate FBP in the muscle (left) and the panel on the right pulse-chase injection to visualize the muscle regions that use glycogen (right). (b) Schematic of anticipated histological features after cryosectioning the muscle. A typical cross-section captures soleus (composed of Type 1 and Type 2a fibers), plantaris (mixed fiber), and gastrocnemius muscles containing mostly Type 2b muscle fibers. (S: soleus, P: plantaris and G: gastrocnemius) (c–e) Serial sections of mouse leg muscles from 2.5 h [U-^{13}C] glucose infusion. (c) Immunohistochemistry to identify muscle fiber type in legs of mice. Red staining indicates fibers positive for anti-MYH7, a marker of type 1 fibers. Green staining indicates fibers positive for anti-MYH2a, a marker of type 2a fibers. Blue staining indicates fibers positive for anti-MYH2b, a marker of Type 2b fibers. (d, e) Metabolite images from short glucose infusion in skeletal muscle. FBP labeling from glucose and NADH levels are distinctly high in the soleus, rich in type 1 muscle fibers as revealed by wash. NADH levels are low in the gastrocnemius. Scale bar: 0.5 mm. (f–h) Serial sections of mouse leg muscles from pulse-chase glucose infusion. (f) Immunohistochemistry to identify muscle fiber type in legs of mice. Red staining indicates fibers positive for anti-MYH7, a marker of type 1 fibers. Green staining indicates fibers positive for anti-MYH2a, a marker of Type 2a fibers. Blue staining indicates fibers positive for anti-MYH2b, a marker of Type 2b fibers. (g, h) Metabolite images from pulse-chase glucose infusion in skeletal muscle. FBP labeling was seen across the tissue regardless of fiber type, indicating glycogen breakdown. Scale bar: 0.5 mm.

NAD^+ in cortex. On the other hand, $^{13}C_6$-NAM comes from circulating blood. Therefore, its level should be the highest in blood vessels followed by medulla and outer stripe based on the proximity to circulating blood. The observed NAD^+ labeling pattern is the combined result of substrate availability and NMNAT expression level. In addition, there is a subtle but consistent trend that the NADH labeling ratio is lower than that of NAD^+, suggesting that NADH is being converted from NAD^+, not vice versa (Figure 2c).

Examination of other nucleotides reveals that the apparent ATP:ADP ratio (based on raw signal intensities) also shows a pattern that distinguishes blood vessels, medulla, outer stripe, and cortex (the latter two being indistinguishable) (Figure 2b). In the case of glucose metabolism, the ATP:ADP ratio impacts the direction of reaction flux through phosphoglycerate kinase, favoring either glycolysis or gluconeogenesis.[33,34] Gluconeogenesis is a process that requires ATP, and the tissue must reserve a sufficient amount of ATP to maintain glucose homeostasis. The higher relative ATP in the renal cortex and lower in medulla is consistent with the fact that the cortex is the leading site of gluconeogenesis in the kidney, while the medulla is the main site of glycolysis.[35]

https://doi.org/10.1021/acs.analchem.3c01875
Anal. Chem. 2023, 95, 14879−14888

Glycolysis in Different Regions and Fiber Types of the Muscle. Because our acidic methanol wash improves the detection of phosphate-containing energy metabolites, we applied this technique to study the metabolic heterogeneity of muscle fibers. Glycolytic metabolites have a low abundance in mammalian tissues, making them harder to detect by conventional and spatial mass spectrometry methods. We hypothesized that our acidic methanol wash approach would be helpful to determine the source of glycolytic intermediates, particularly those that are phosphorylated. Recent work in mice has shown that different muscles in the leg use diverse nutrient pools to feed glycolysis.[36] The soleus muscle, rich in Type 1 and Type 2a muscle fibers, primarily uses circulating glucose for glycolysis. In contrast, the gastrocnemius muscle, rich in Type 2b fibers, primarily uses glycogen stored within the tissue.[36] However, these studies have used LC−MS to measure these differences in metabolites in bulk tissue and ignored the heterogeneity of fibers in these muscles. In particular, the inner region of the gastrocnemius muscle has more Type 2a or Type 1 muscle fibers, a part classically known as the red gastrocnemius. We hypothesized that the fiber composition of individual muscle types would rely differentially on circulating glucose compared to stored glycogen to power glycolysis.

Using our optimized acidic methanol wash, we aimed to determine whether different fiber types within the gastrocnemius muscle use alternative substrates for glycolysis. To visualize the muscle regions that directly use circulating glucose for glycolysis, we performed a 2.5-hour infusion of U-^{13}C-glucose. We visualized labeling in glycolytic intermediate FBP in the muscle (Figure 3a,b). Consistent with our prior publication, fully labeled FBP was high in the soleus muscle and low in the gastrocnemius muscle regions rich in Type 2b fibers. However, within the red gastrocnemius muscle with more type 2a and type 1 muscle fibers, the labeling was higher than in the other region of the gastrocnemius muscle. In addition, the plantaris muscle, composed of all fiber types, showed similar labeling to the red gastrocnemius regions (Figure 3c,d). Importantly, our acidic methanol wash enabled the visualization of regional differences in metabolism.

To visualize the muscle regions that use glycogen (a polymer of glucose stored in muscle) as the direct substrate of glycolysis, we utilized an experimental paradigm in which we can label glycogen pools by pulse-chase infusions. This allows us to trace carbons coming out of the glycogen pool. To label the glycogen pools in the tissue, U-^{13}C-glucose was infused during the dark cycle while mice ate food ad-lib. Then, to reduce the labeling of circulating glucose, we stopped the infusion during the light process. After 4 h of no infusion, the glycogen in the tissue remains labeled while circulating glucose is only minimally labeled (Figure S10). At the end of the pulse-chase, we visualized labeling in FBP and observed abundant m + 6 labeling across the tissue regardless of fiber type (Figure 3f,g). Because the gastrocnemius regions rich in type 2b fibers did not label from 2.5 h glucose infusion but did label when glycogen was labeled by pulse-chase, we conclude that the labeling within this tissue comes from glycogen. This confirms that these regions of the gastrocnemius muscle use glycogen rather than circulating glucose for glycolysis.

We could visualize high levels of NADH in the soleus, which uses glucose for glycolysis (Figure 3e,h). High NADH levels correlate with high glycolytic flux. Conversely, when the glycolytic flux is low, many glycolytic enzymes are near equilibrium and exhibit reversibility.[37] This can be detected by reversibility in the aldolase reaction, resulting in the m + 3 labeling of FBP. The soleus was low in m + 3 labeling of FBP relative to the other muscles in the 2.5 h and pulse-chase glucose infusions (Figure S10). Combined, these data suggest high glycolytic flux from circulating glucose in the soleus muscle and relatively lower glycolytic flux in other leg muscles.

DISCUSSION

Challenges for MALDI-MSI include improving molecular coverage. The combination of our approaches enables detection of ∼220 mammalian metabolites involved in central metabolism: ∼170 metabolites in negative mode with the NEDC matrix and ∼80 metabolites in positive mode with the THAP matrix (Table S7). Improving metabolite detection sensitivity will facilitate using small raster sizes for better spatial resolution. Indeed, Korte et al. revealed that the molecular distribution of metabolites and lipids might be heterogeneous even among cells of the same tissue type, posing the problem of inefficient detection of metabolites due to ion suppression.[38] We show that washing with organic solvents such as chloroform can remove lipids, increasing the signal for many polar metabolites. In addition, washing with acidic methanol can effectively remove lipids and highly polar metabolites such as amino acids and denaturing proteins, enhancing the detection of phosphate-containing energy metabolites while maintaining histological integrity. On-slide derivatization is a complementary approach[39,40] and could further enhance the signal if performed either before or after a wash step. This improved detection of cellular metabolites through multiple improvements in sample preparation will contribute to imaging mass spectrometry with better spatial resolution, eventually reaching the single-cell level.[41]

Capturing the energetic status (e.g., ATP:ADP ratio) can provide insight into tissue function and health, such as tissue age or perfusion.[42,43] Currently, our methods provide enhanced signal intensity for ATP and ADP, facilitating measuring their relative signals. But these signals may be impacted by ATP degradation during tissue processing or in-source fragmentation of ATP (including into ADP). We also do not yet provide absolute quantitation. Further research is needed. We anticipate that these ratios, if understood spatially in the baseline condition, could provide significant value to assessing animal models of disease (e.g., kidney disease, cancer, neurological diseases).[34] For example, cancer cells are characterized by enhanced aerobic glycolysis that may lead to a different ATP:ADP ratio than normal cells.[44,45] Thus, if performed during biopsy, these could lead to classification of disease progression or treatment response.

Our work also has substantial implications for lipidomics and metabolomics regarding metabolite extraction from biological samples. Our initial screen of different solvents for polar metabolite detection shows that chloroform effectively removes lipids from tissue sections. This suggests that chloroform is a suitable solvent for extracting lipids from tissue samples.[46,47] For polar metabolite extraction, an important consideration is that many metabolites bind with proteins.[48,49] To effectively extract these protein-bound metabolites, it may be useful to denature the proteins, which can be achieved using a variety of approaches, such as the use of acid, detergent, or heat.[23,50−54] For mass spectrometry imaging, it will be interesting to explore other approaches that denature proteins and enhance SMM detection while also maintaining histological integrity, in

https://doi.org/10.1021/acs.analchem.3c01875
Anal. Chem. 2023, 95, 14879−14888

addition to the acidic methanol treatment we developed in this study.

CONCLUSIONS

Improving sensitivity is a primary challenge for MALDI imaging of small molecule metabolites. Here, we developed an approach that involves treating tissues with acidic methanol to improve the detection of metabolites involved in energy metabolism, specifically phosphate-containing metabolites. We demonstrate that this solvent wash strategy improves the ionization efficiency of these metabolites by denaturing proteins, removing lipids, and removing other highly polar metabolites that cause ion suppression of target polar analytes. Combining this solvent wash strategy with isotope tracing holds the potential for a better empirical and mechanistic understanding of the ionization of metabolites in mammalian tissues. More broadly, improving metabolome coverage using MALDI will lead to important biological discoveries.

ASSOCIATED CONTENT

Data Availability Statement

All relevant data are presented in the Supporting Information. MALDI-MSI data files for mouse brain sections at 50 μm spatial resolution under various wash conditions were deposited at https://massive.ucsd.edu/ with accession ID MSV000092611. Additional data and reagents are available upon reasonable request.

Supporting Information

The Supporting Information is available free of charge at https://pubs.acs.org/doi/10.1021/acs.analchem.3c01875.

Supporting information of chemicals and reagents, animal infusions, matrix coating, Immunofluorescence, H&E staining, BCA total protein assay and native PAGE gel, on-tissue MALDI-MS/MS, and sample processing for LC−MS; figures of different wash procedures explored, additional results of mouse brain and kidney before and after washing with 13 solvents, results of 3-PG, hexose-6P, FBP, AMP, ADP, and ATP after treatment with different volumes of MeOH + 0.5% FA, MeOH + 0.05% FA, and MeOH + 0.1% FA, densitometry profile of samples before and after treatments with methanol or methanol+0.05% FA, MALDI mass spectra of mouse brain sections from control, or after treatment with chloroform, methanol, or methanol + 0.05% FA, LC−MS analysis of the post-wash solvents, LC−MS chromatograms of NAD^+, NADH, $NADP^+$, NADPH, ATP, and ADP from a mouse kidney extract, additional results for mouse muscle labeling experiments; Supporting Tables of physical and chemical properties of 13 solvents used in the initial evaluation, fold of difference for selected metabolites after washing with 13 solvents, fold of difference for selected metabolites after washing with acetonitrile, methanol, H_2O, and formic acid (FA) combinations, on tissue MS2 results for 21 metabolites (PDF)

Signal intensity for ∼100 polar metabolites and 41 lipids from mouse brain and kidney before and after wash with 13 different solvents (XSLX)

List of 175 compounds in negative mode with NEDC matrix and 80 compounds in positive mode with THAP matrix (XSLX)

Signal intensity of 175 compounds in negative mode with NEDC matrix and 80 compounds in positive mode with THAP matrix from mouse brain, kidney, muscle, spleen, and heart under four conditions: (1) no wash control, (2) wash with 5 mL of chloroform, (3) 5 mL of MeOH, and (4) 5 mL of MeOH + 0.05% FA (XSLX)

Lock masses used in negative mode with NEDC matrix and positive mode with THAP matrix (XSLX)

AUTHOR INFORMATION

Corresponding Authors

Wenyun Lu − *Lewis Sigler Institute for Integrative Genomics, Princeton University, Princeton, New Jersey 08544, United States; Department of Chemistry, Princeton University, Princeton, New Jersey 08544, United States;* orcid.org/0000-0003-1787-2617; Email: wlu@princeton.edu

Shawn M. Davidson − *Lewis Sigler Institute for Integrative Genomics, Princeton University, Princeton, New Jersey 08544, United States; Rutgers Cancer Institute of New Jersey (CINJ), Rutgers University, New Brunswick, New Jersey 08901, United States;* orcid.org/0000-0002-3475-0382; Email: shawnd@princeton.edu

Authors

Noel R. Park − *Lewis Sigler Institute for Integrative Genomics, Princeton University, Princeton, New Jersey 08544, United States*

Tara TeSlaa − *Department of Molecular and Medical Pharmacology, University of California Los Angeles, Los Angeles, California 90095, United States*

Connor S.R. Jankowski − *Lewis Sigler Institute for Integrative Genomics, Princeton University, Princeton, New Jersey 08544, United States*

Laith Samarah − *Lewis Sigler Institute for Integrative Genomics, Princeton University, Princeton, New Jersey 08544, United States*

Melanie McReynolds − *Department of Biochemistry and Molecular Biology, The Pennsylvania State University, University Park, Pennsylvania 16802, United States*

Xi Xing − *Lewis Sigler Institute for Integrative Genomics, Princeton University, Princeton, New Jersey 08544, United States; Department of Chemistry, Princeton University, Princeton, New Jersey 08544, United States*

Jessica Schembri − *Lewis Sigler Institute for Integrative Genomics, Princeton University, Princeton, New Jersey 08544, United States*

Morgan T. Woolf − *Department of Systems Pharmacology and Translational Therapeutics, University of Pennsylvania, Philadelphia, Pennsylvania 19104, United States*

Joshua D. Rabinowitz − *Lewis Sigler Institute for Integrative Genomics, Princeton University, Princeton, New Jersey 08544, United States; Rutgers Cancer Institute of New Jersey (CINJ), Rutgers University, New Brunswick, New Jersey 08901, United States; Department of Chemistry and Ludwig Institute for Cancer Research, Princeton University, Princeton, New Jersey 08544, United States;* orcid.org/0000-0002-1247-4727

Complete contact information is available at: https://pubs.acs.org/10.1021/acs.analchem.3c01875

Author Contributions

Conceptualization: W.L., S.M.D.; methodology: W.L., N.R.P., T.TS., C.S.R.J., L.S., M.M., X.X., J.S., M.W.; formal analysis and investigation: W.L., N.R.P., S.M.D.; writing − original draft preparation: W.L., N.R.P., T.TS., S.M.D.; writing − review and

https://doi.org/10.1021/acs.analchem.3c01875
Anal. Chem. 2023, 95, 14879−14888

editing: W.L., S.M.D.; funding acquisition: W.L., S.M.D., J.D.R.; resources: W.L., S.M.D., J.D.R.; supervision: S.M.D., J.D.R.

Notes

The authors declare the following competing financial interest(s): J.D.R. is an advisor and stockholder in Colorado Research Partners, Empress Therapeutics, and Marea Therapeutics; a consultant of Pfizer and Third Rock Ventures; a founder, director, and stockholder of Farber Partners, Serien Therapeutics, and Sofro Pharmaceuticals; inventor of patents held by Princeton University; and a director of the Princeton University-PKU Shenzhen collaboration.

■ ACKNOWLEDGMENTS

We thank members of the Davidson and Rabinowitz labs for help and discussion. This work was supported by the Paul G. Allen Family Foundation grant 0034665 (S.M.D. and J.D.R.), the Rutgers Cancer Institute of New Jersey Center Grant P30CA072720 (J.D.R.), the UPenn Diabetes Research Center grant P30DK019525 (J.D.R.), the Calico Life Sciences Company (J.D.R.), NIH grant R50CA211437 (W.L.), NIH grant 1-RF1-AG075901-01A1, the Howard Hughes Medical Institute Hanna H. Gray Fellows Program Faculty Phase grant GT15655 (M.R.M), the Burroughs Wellcome Fund PDEP Transition to Faculty grant 1022604 (M.R.M), Stand Up 2 Cancer Convergence 3.146 (S.M.D. and J.D.R.), and the Cystinosis Research Foundation (S.M.D.).

■ REFERENCES

(1) Alexandrov, T. *Annu. Rev. Biomed. Data Sci.* **2020**, *3*, 61.
(2) Ivanisevic, J.; Epstein, A. A.; Kurczy, M. E.; Benton, P. H.; Uritboonthai, W.; Fox, H. S.; Boska, M. D.; Gendelman, H. E.; Siuzdak, G. *Chem. Biol.* **2014**, *21*, 1575.
(3) Ding, J.; Ji, J.; Rabow, Z.; Shen, T.; Folz, J.; Brydges, C. R.; Fan, S.; Lu, X.; Mehta, S.; Showalter, M. R.; Zhang, Y.; Araiza, R.; Bower, L. R.; Lloyd, K. C. K.; Fiehn, O. *Nat. Commun.* **2021**, *12*, 021.
(4) Pang, H.; Li, J.; Hu, X.; Chen, F.; Gao, X.; Zacharias, L. G.; Cai, F.; DeBerardinis, R. J.; Sun, W.; Hu, Z.; Ge, W. *bioRxiv* **2020**, DOI: 10.1101/2020.12.28.424544.
(5) Norris, J. L.; Caprioli, R. M. *Chem. Rev.* **2013**, *113*, 2309.
(6) Buchberger, A. R.; DeLaney, K.; Johnson, J.; Li, L. *Anal. Chem.* **2018**, *90*, 240.
(7) Arts, M.; Soons, Z.; Ellis, S. R.; Pierzchalski, K. A.; Balluff, B.; Eijkel, G. B.; Dubois, L. J.; Lieuwes, N. G.; Agten, S. M.; Hackeng, T. M.; van Loon, L. J. C.; Heeren, R. M. A.; Olde Damink, S. W. M. *Angew. Chem., Int. Ed. Engl.* **2017**, *56*, 7146.
(8) Wang, L.; Xing, X.; Zeng, X.; Jackson, S. R.; TeSlaa, T.; Al-Dalahmah, O.; Samarah, L. Z.; Goodwin, K.; Yang, L.; McReynolds, M. R.; Li, X.; Wolff, J. J.; Rabinowitz, J. D.; Davidson, S. M. *Nat. Methods* **2022**, *19*, 223.
(9) Bartman, C. R.; TeSlaa, T.; Rabinowitz, J. D. *Nat. Metab.* **2021**, *3*, 896.
(10) Bartman, C. R.; Weilandt, D. R.; Shen, Y.; Lee, W. D.; Han, Y.; TeSlaa, T.; Jankowski, C. S. R.; Samarah, L.; Park, N. R.; da Silva-Diz, V.; Aleksandrova, M.; Gultekin, Y.; Marishta, A.; Wang, L.; Yang, L.; Roichman, A.; Bhatt, V.; Lan, T.; Hu, Z.; Xing, X.; Lu, W.; Davidson, S.; Wuhr, M.; Vander Heiden, M. G.; Herranz, D.; Guo, J. Y.; Kang, Y.; Rabinowitz, J. D. *Nature* **2023**, *614*, 349.
(11) Lemaire, R.; Wisztorski, M.; Desmons, A.; Tabet, J. C.; Day, R.; Salzet, M.; Fournier, I. *Anal. Chem.* **2006**, *78*, 7145.
(12) Seeley, E. H.; Oppenheimer, S. R.; Mi, D.; Chaurand, P.; Caprioli, R. M. *J. Am. Soc. Mass Spectrom.* **2008**, *19*, 1069.
(13) Yang, J.; Caprioli, R. M. *Anal. Chem.* **2011**, *83*, 5728.
(14) Patterson, N. H.; Thomas, A.; Chaurand, P. *J. Mass. Spectrom.* **2014**, *49*, 622.
(15) Yang, H.; Ji, W.; Guan, M.; Li, S.; Zhang, Y.; Zhao, Z.; Mao, L. *Metabolomics* **2018**, *14*, 50.
(16) Sun, C.; Li, Z.; Ma, C.; Zang, Q.; Li, J.; Liu, W.; Zhao, H.; Wang, X. *J. Pharm. Biomed. Anal.* **2019**, *176*, No. 112797.
(17) Angel, P. M.; Spraggins, J. M.; Baldwin, H. S.; Caprioli, R. *Anal. Chem.* **2012**, *84*, 1557.
(18) Hui, S.; Cowan, A. J.; Zeng, X.; Yang, L.; TeSlaa, T.; Li, X.; Bartman, C.; Zhang, Z.; Jang, C.; Wang, L.; Lu, W.; Rojas, J.; Baur, J.; Rabinowitz, J. D. *Cell Metab.* **2020**, *32*, 676.
(19) Wang, L.; Xing, X.; Chen, L.; Yang, L.; Su, X.; Rabitz, H.; Lu, W.; Rabinowitz, J. D. *Anal. Chem.* **1838**, *2019*, 91.
(20) Lu, W.; Xing, X.; Wang, L.; Chen, L.; Zhang, S.; McReynolds, M. R.; Rabinowitz, J. D. *Anal. Chem.* **2020**, *92*, 11573.
(21) Chen, L.; Lu, W.; Wang, L.; Xing, X.; Chen, Z.; Teng, X.; Zeng, X.; Muscarella, A. D.; Shen, Y.; Cowan, A.; McReynolds, M. R.; Kennedy, B. J.; Lato, A. M.; Campagna, S. R.; Singh, M.; Rabinowitz, J. D. *Nat. Methods* **2021**, *18*, 1377.
(22) Lu, W.; Wang, L.; Chen, L.; Hui, S.; Rabinowitz, J. D. *Antioxid. Redox Signaling* **2018**, *28*, 167.
(23) Lu, W.; Su, X.; Klein, M. S.; Lewis, I. A.; Fiehn, O.; Rabinowitz, J. D. *Annu. Rev. Biochem.* **2017**, *86*, 277.
(24) Bruce, K. D.; Zsombok, A.; Eckel, R. H. *Front. Endocr.* **2017**, *8*, 60.
(25) Chauhan, J. S.; Mishra, N. K.; Raghava, G. P. *BMC Bioinf.* **2009**, *10*, 1471.
(26) Hua, Y. H.; Wu, C. Y.; Sargsyan, K.; Lim, C. *Sci. Rep.* **2014**, *4*, 6471.
(27) Bonora, M.; Patergnani, S.; Rimessi, A.; De Marchi, E.; Suski, J. M.; Bononi, A.; Giorgi, C.; Marchi, S.; Missiroli, S.; Poletti, F.; Wieckowski, M. R.; Pinton, P. *Purinergic Signal.* **2012**, *8*, 343.
(28) Stein, L. R.; Imai, S. *Trends Endocr. & Metab.* **2012**, *23*, 420.
(29) Xiao, W.; Wang, R. S.; Handy, D. E.; Loscalzo, J. *Antioxid. Redox Signaling* **2018**, *28*, 251.
(30) Liu, L.; Su, X.; Quinn, W. J., 3rd; Hui, S.; Krukenberg, K.; Frederick, D. W.; Redpath, P.; Zhan, L.; Chellappa, K.; White, E.; Migaud, M.; Mitchison, T. J.; Baur, J. A.; Rabinowitz, J. D. *Cell Metab.* **2018**, *27*, 1067.
(31) Ralto, K. M.; Rhee, E. P.; Parikh, S. M. *Nat. Rev. Nephr.* **2020**, *16*, 99.
(32) McReynolds, M. R.; Chellappa, K.; Chiles, E.; Jankowski, C.; Shen, Y.; Chen, L.; Descamps, H. C.; Mukherjee, S.; Bhat, Y. R.; Lingala, S. R.; Chu, Q.; Botolin, P.; Hayat, F.; Doke, T.; Susztak, K.; Thaiss, C. A.; Lu, W.; Migaud, M. E.; Su, X.; Rabinowitz, J. D.; Baur, J. A. *Cell Syst.* **2021**, *12*, 1160.
(33) Veech, R. L.; Lawson, J. W.; Cornell, N. W.; Krebs, H. A. *J. Biol. Chem.* **1979**, *254*, 6538.
(34) Tantama, M.; Martínez-François, J. R.; Mongeon, R.; Yellen, G. *Nat. Commun.* **2013**, *4*, 2550.
(35) Castellino, P.; DeFronzo, R. A. *Semin. Nephr.* **1990**, *10*, 458.
(36) TeSlaa, T.; Bartman, C. R.; Jankowski, C. S. R.; Zhang, Z.; Xu, X.; Xing, X.; Wang, L.; Lu, W.; Hui, S.; Rabinowitz, J. D. *Cell Metab.* **2021**, *33*, 367.
(37) Park, J. O.; Tanner, L. B.; Wei, M. H.; Khana, D. B.; Jacobson, T. B.; Zhang, Z.; Rubin, S. A.; Li, S. H.; Higgins, M. B.; Stevenson, D. M.; Amador-Noguez, D.; Rabinowitz, J. D. *Nat. Chem. Biol.* **2019**, *15*, 1001.
(38) Korte, A. R.; Yandeau-Nelson, M. D.; Nikolau, B. J.; Lee, Y. J. *Anal. Bioanal. Chem.* **2015**, *407*, 2301.
(39) Dueñas, M. E.; Larson, E. A.; Lee, Y. J. *Plant Sci.* **2019**, *10*, 860.
(40) Kaya, I.; Schembri, L. S.; Nilsson, A.; Shariatgorji, R.; Baijnath, S.; Zhang, X.; Bezard, E.; Svenningsson, P.; Odell, L. R.; Andrén, P. E. *J. Am. Soc. Mass Spectrom.* **2023**, *34*, 836.
(41) Rappez, L.; Stadler, M.; Triana, S.; Gathungu, R. M.; Ovchinnikova, K.; Phapale, P.; Heikenwalder, M.; Alexandrov, T. *Nat. Methods* **2021**, *18*, 799.
(42) Ghosh, A.; Ronner, P.; Cheong, E.; Khalid, P.; Matschinsky, F. M. *J. Biol. Chem.* **1991**, *266*, 22887.
(43) Martin, J. L.; Costa, A. S. H.; Gruszczyk, A. V.; Beach, T. E.; Allen, F. M.; Prag, H. A.; Hinchy, E. C.; Mahbubani, K.; Hamed, M.; Tronci, L.; Nikitopoulou, E.; James, A. M.; Krieg, T.; Robinson, A. J.; Huang, M. M.; Caldwell, S. T.; Logan, A.; Pala, L.; Hartley, R. C.; Frezza, C.; Saeb-Parsy, K.; Murphy, M. P. *Nat. Metab.* **2019**, *1*, 966.

(44) Lunt, S. Y.; Vander Heiden, M. G. *Annu. Rev. Cell Dev. Biol.* **2011**, *27*, 441.
(45) Maldonado, E. N.; Lemasters, J. J. *Mitochondrion* **2014**, *19*, 78.
(46) Folch, J.; Lees, M.; Sloane Stanley, G. H. *J. Biol. Chem.* **1957**, *226*, 497.
(47) Bligh, E. G.; Dyer, W. J. *Can. J. Biochem. Physiol.* **1959**, *37*, 911.
(48) Bennett, B. D.; Kimball, E. H.; Gao, M.; Osterhout, R.; Van Dien, S. J.; Rabinowitz, J. D. *Nat. Chem. Biol.* **2009**, *5*, 593.
(49) Piazza, I.; Kochanowski, K.; Cappelletti, V.; Fuhrer, T.; Noor, E.; Sauer, U.; Picotti, P. *Cell* **2018**, *172*, 358.
(50) Alseekh, S.; Aharoni, A.; Brotman, Y.; Contrepois, K.; D'Auria, J.; Ewald, J.; Ewald, J. C.; Fraser, P. D.; Giavalisco, P.; Hall, R. D.; Heinemann, M.; Link, H.; Luo, J.; Neumann, S.; Nielsen, J.; Perez de Souza, L.; Saito, K.; Sauer, U.; Schroeder, F. C.; Schuster, S.; Siuzdak, G.; Skirycz, A.; Sumner, L. W.; Snyder, M. P.; Tang, H.; Tohge, T.; Wang, Y.; Wen, W.; Wu, S.; Xu, G.; Zamboni, N.; Fernie, A. R. *Nat. Methods* **2021**, *18*, 747.
(51) Tennessen, J. M.; Barry, W. E.; Cox, J.; Thummel, C. S. *Methods* **2014**, *68*, 105.
(52) Moreira, J. D.; Hamraz, M.; Abolhassani, M.; Bigan, E.; Pérès, S.; Paulevé, L.; Nogueira, M. L.; Steyaert, J. M.; Schwartz, L. *Metabolites* **2016**, *6*, 33.
(53) Gonzalez, B.; François, J.; Renaud, M. *Yeast* **1997**, *13*, 1347.
(54) Trefely, S.; Liu, J.; Huber, K.; Doan, M. T.; Jiang, H.; Singh, J.; von Krusenstiern, E.; Bostwick, A.; Xu, P.; Bogner-Strauss, J. G.; Wellen, K. E.; Snyder, N. W. *Mol. Metab.* **2019**, *30*, 61.

https://doi.org/10.1021/acs.analchem.3c01875
Anal. Chem. 2023, 95, 14879−14888